

## Article

# The Potential Cytotoxic Activity Enhancement of $\alpha$ -Mangostin in Chitosan-Kappa Carrageenan-Loaded Nanoparticle against MCF-7 Cell Line

Nasrul Wathoni <sup>1,\*</sup> , Lisna Meylina <sup>1,2</sup>, Agus Rusdin <sup>1,3</sup>, Ahmed Fouad Abdelwahab Mohammed <sup>4</sup> , Dorandani Tirtamie <sup>1</sup>, Yedi Herdiana <sup>1</sup>, Keiichi Motoyama <sup>5</sup> , Camelia Panatarani <sup>6,7</sup>, I Made Joni <sup>6,7</sup>, Ronny Lesmana <sup>8</sup> and Muchtaridi Muchtaridi <sup>9</sup> 

- <sup>1</sup> Department of Pharmaceutics and Pharmaceutical Technology, Faculty of Pharmacy, Universitas Padjadjaran, Sumedang 45363, Indonesia; lisna@farmasi.unmul.ac.id (L.M.); agusrusdin@gmail.com (A.R.); farmasetikers@gmail.com (D.T.); y.herdiana@unpad.ac.id (Y.H.)
  - <sup>2</sup> Department of Pharmaceutics and Pharmaceutical Technology, Faculty of Pharmacy, Universitas Mulawarman, Samarinda 75119, Indonesia
  - <sup>3</sup> Department of Pharmacy, Faculty of Sports and Health, Universitas Negeri Gorontalo, Gorontalo 96128, Indonesia
  - <sup>4</sup> Department of Pharmaceutics, Faculty of Pharmacy, Minia University, Minia 61519, Egypt; ahmed.mohamed1@minia.edu.eg
  - <sup>5</sup> Graduate School of Pharmaceutical Sciences, Kumamoto University, Kumamoto 862-0973, Japan; motoyama@kumamoto-u.ac.jp
  - <sup>6</sup> Department of Physics, Faculty of Mathematics and Natural Sciences, Universitas Padjadjaran, Sumedang 45363, Indonesia; c.panatarani@unpad.ac.id (C.P.); imadejoni@phys.unpad.ac.id (I.M.J.)
  - <sup>7</sup> Functional Nano Powder University Center of Excellence, Universitas Padjadjaran, Sumedang 45363, Indonesia
  - <sup>8</sup> Department of Anatomy, Physiology and Biology Cell, Faculty of Medicine, Universitas Padjadjaran, Sumedang 45363, Indonesia; ronny@unpad.ac.id
  - <sup>9</sup> Department of Pharmaceutical Analysis and Medicinal Chemistry, Faculty of Pharmacy, Universitas Padjadjaran, Sumedang 45363, Indonesia; muchtaridi@unpad.ac.id
- \* Correspondence: nasrul@unpad.ac.id; Tel.: +62-22-842-888888 (ext. 3510)



**Citation:** Wathoni, N.; Meylina, L.; Rusdin, A.; Mohammed, A.F.A.; Tirtamie, D.; Herdiana, Y.; Motoyama, K.; Panatarani, C.; Joni, I.M.; Lesmana, R.; et al. The Potential Cytotoxic Activity Enhancement of  $\alpha$ -Mangostin in Chitosan-Kappa Carrageenan-Loaded Nanoparticle against MCF-7 Cell Line. *Polymers* **2021**, *13*, 1681. <https://doi.org/10.3390/polym13111681>

Academic Editors: Dimitrios Bikiaris and Barbara Viganì

Received: 13 March 2021  
Accepted: 18 May 2021  
Published: 21 May 2021

**Publisher's Note:** MDPI stays neutral with regard to jurisdictional claims in published maps and institutional affiliations.



**Copyright:** © 2021 by the authors. Licensee MDPI, Basel, Switzerland. This article is an open access article distributed under the terms and conditions of the Creative Commons Attribution (CC BY) license (<https://creativecommons.org/licenses/by/4.0/>).

**Abstract:**  $\alpha$ -mangostin ( $\alpha$ M), a xanthone derivative compound isolated from the extract of mangosteen pericarp (*Garcinia mangostana* L), has potential anticancer properties for breast cancer. However, it has poor solubility in water and low selectivity towards cancer cells. The polymeric nanoparticle formulation approach can be used to overcome these problems. In this study, a chitosan biopolymer-based  $\alpha$ M polymeric nanoparticle formulation was encapsulated using kappa carrageenan ( $\alpha$ M-Ch/Cr) as a novel carrier for breast cancer therapy and evaluated for their physicochemical properties, drug release profile, and in vitro cytotoxicity against breast cancer cells (MCF-7). Polymeric nanoparticles formulated with varying concentrations of kappa carrageenan were successfully prepared by ionic gelation and spray pyrolysis techniques.  $\alpha$ M-Ch/Cr nanoparticles formed perfectly round particles with a size of 200–400 nm and entrapment efficiency  $\geq 98\%$ . In vitro release studies confirmed that  $\alpha$ M-Ch/Cr nanoparticles had a sustained release system profile. Interestingly, the formulation of polymeric nanoparticles significantly ( $p < 0.05$ ) increased the cytotoxicity of  $\alpha$ M against MCF-7 cell with IC<sub>50</sub> value of 4.7  $\mu$ g/mL compared to the non-nanoparticle with IC<sub>50</sub> of 8.2  $\mu$ g/mL. These results indicate that  $\alpha$ M-Ch/Cr nanoparticles have the potential to improve the physicochemical properties and cytotoxicity effects of  $\alpha$ M compounds as breast cancer therapy agents.

**Keywords:** chitosan; cytotoxic; kappa carrageenan;  $\alpha$ -mangostin; polymeric nanoparticle

## 1. Introduction

Breast cancer is the second most prevalent cancer after lung cancer, accounting for 11.6% of all cancer cases (2,088,849 cases) and 6.6% of all cancer-related deaths (626,679 deaths)

in 2018 [1]. Breast cancer is currently treated with local treatment (surgery and radiation) and systemic treatment (chemotherapy, hormone therapy, targeted drug therapy, and immunotherapy) [2]. However, these therapeutic methods have many side effects. Besides, the efficacy of chemotherapeutic agents is also reduced by the presence of cancer cell resistance (multi-drug resistance mechanism) [3,4].

Nowadays, natural ingredients are mostly used for alternative cancer treatment.  $\alpha$ -mangostin ( $\alpha$ M), a secondary metabolite isolated from pericarp of mangosteen (*Garcinia mangostana* Linn), had been reported to have a potent cytotoxic effect by induction of apoptosis in various cancer cell lines [5].  $\alpha$ M induced apoptosis in breast cancer cells through the inhibition of fatty acid synthase via the signaling pathway of human epidermal growth factor receptor-2 (HER2)/phosphatidylinositide 3-kinase (PI3K)/Akt and mitogen-activated protein kinase (MAPK). Despite its potent cytotoxic effect and anticancer activity,  $\alpha$ M has limitations in physicochemical properties that need to be considered, including low solubility and its non-selectivity to cancer cells [6,7]. These properties reduce its effectiveness in treatment of cancer.

In a polymeric nanoparticle drug delivery system, nanoparticles are utilized as drug carriers. Some studies suggest that the use of polymeric nanoparticles as a drug delivery system can increase drug solubility, provide a controlled drug release, and accumulate in cancer tissues through enhanced permeability and retention effect (EPR), allowing for more specific targeting [8–11]. Chitosan, a biopolymer obtained by alkaline deacetylation of chitin, has properties as a promising material for nanoparticle drug delivery [12–14]. The mucoadhesive properties of chitosan can increase drug penetration into cancer cells and suppress drug efflux reactions to maximize the level of drug entering the cells. In addition, chitosan nanoparticles can inhibit cell migration activity in MDA-MB-231 [15], and improve anticancer activities in HeLa [16], HUVE [17], and HCC cells [18]. The activities of chitosan in killing cancer cells are known to work through the mechanism of induction of apoptosis through activation of caspases 3, 8, 9; modulation ratio of Bax: Bcl-2; induce DNA damage [19,20] and the characteristics of chitosan undergo protonation in acidic environments and provide useful release at low pH as in tumor microenvironment that has acidic pH [21]. However, in oral administration, this activity can decrease due to the protonation of the amine group of chitosan [22–24].

Enteric-coated nanoparticles are one of the drug delivery systems in oral administration that can protect the reaction of degradation and control the release of encapsulated drugs in specific parts of the gastrointestinal tract. Kappa carrageenan is often used as a coating material because of its low sensitivity to pH and ionic strength [25]. Owing to its negative charge, kappa carrageenan is commonly used in combination with cationic or polymeric cationic polymerized electrolytes as a microcapsule shell. Kappa carrageenan is also used together with chitosan in the manufacture of microcapsules containing glucose oxidase for controlled release for oral administration [26] and nanoparticles containing recombinant human erythropoietin [27], ciprofloxacin [28], and  $\text{SiO}_2\text{-NH}_2$  [29].

Following a review of the literature, there are no studies reported using chitosan polymeric nanoparticles loaded with kappa carrageenan as a drug delivery system for  $\alpha$ M. Therefore, the main objective of this study was to prepare and characterize  $\alpha$ M nanoparticles, for improving the solubility and anticancer activity of  $\alpha$ M mediated by nanoparticle drug delivery system.

Therefore, the main objective of this study was to prepare the nanoparticle drug delivery system for the oral route of administration. Chitosan, the main carrier for providing solubility and penetration improvement, is known to have instability at gastric pH, therefore, it was added with carrageenan as an encapsulator for protecting chitosan protonation from the gastric fluid (Figure 1). In addition, the physicochemical characterization of the nanoparticle system will characterize and evaluate the release profile of nanoparticles in fluids with different pHs (1.2 and 7.4) for representing gastrointestinal tract condition especially in stomach (pH 1.2) and ileum (pH 7.4). Furthermore, the cytotoxic assay was

studied on breast cancer (MCF-7 cell lines) to evaluate the  $\alpha$ M polymeric nanoparticle cytotoxic effect.

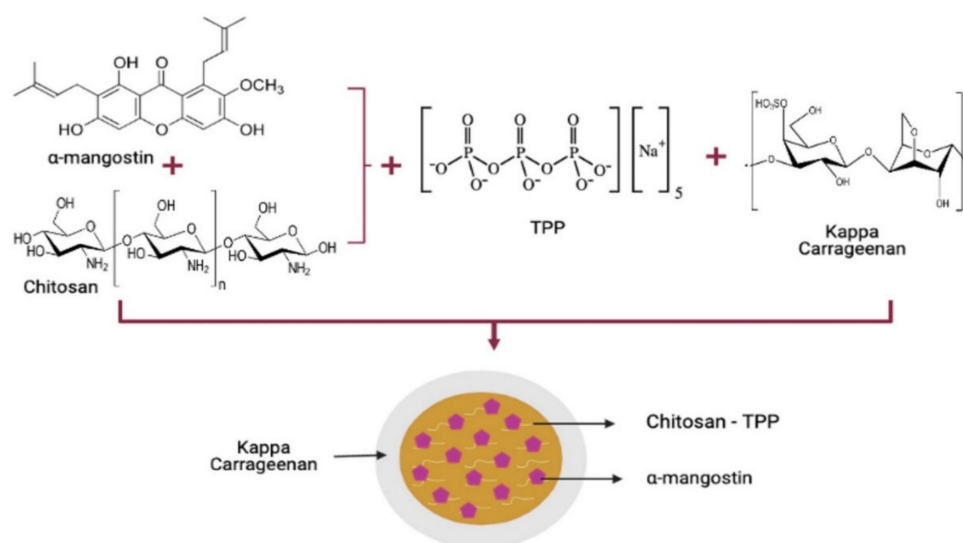


**Figure 1.** Synthesis of  $\alpha$ M chitosan-kappa carrageenan nanoparticles.

## 2. Materials and Methods

### 2.1. Material

$\alpha$ -mangostin ( $\alpha$ M) was purchased from Chengdu Biopurify Phytochemicals (Chengdu, Sichuan, China). Chitosan was isolated with a purity of 70% (MW: 1526.5 g/mol, DD: 81.38%). Sodium tripolyphosphate and kappa carrageenan (MW: 788.7 g/mol) were purchased from Kappa Carrageenan Nusantara (Bekasi, West Java, Indonesia), ethanol from Kristata (Bandung, West Java, Indonesia), and acetic acid solvent from Brataco (Bandung, West Java, Indonesia). MCF-7 human breast cancer cell line was purchased from the American Type Culture Collection (Manassas, VA, USA).

### 2.2. Preparation of $\alpha$ M Chitosan Nanoparticles

The  $\alpha$ M chitosan ( $\alpha$ M-Ch) nanoparticles was prepared by the ionic gelation method. Briefly, 20 mg  $\alpha$ -mangostin was diluted in 20 mL ethanol. Then, it was mixed with 0.1% *w/v* (200 mg/200 mL) of chitosan solution prepared in 1% acetic acid. Next, 0.1% *w/v* (40 mg/40 mL) sodium tripolyphosphate solution was added drop wise under constant magnetic stirring. Then, the system was ultrasonicated for 30 min to reduce the droplet size in the suspension system [30].

### 2.3. Preparation of $\alpha$ M Chitosan-Loaded Kappa Carrageenan Nanoparticles

The  $\alpha$ M chitosan-loaded kappa carrageenan ( $\alpha$ M-Ch/Cr) nanoparticles were prepared by the solvent evaporation method. For the coating process,  $\alpha$ M-Ch was dropped into varying concentrations of kappa carrageenan (F1: 25 mg/25 mL, F2: 45 mg/45 mL, and F3: 85 mg/85 mL) (Table 1). The solution mixture was conducted via microvolume flow titration method, and then, dried nanoparticles were obtained by drying the suspension solutions using spray pyrolysis at a temperature of 80–100 °C and at airflow of 5 L/min [30].

**Table 1.**  $\alpha$ M polymeric nanoparticle formulation.

Formulation	F1	F2	F3
$\alpha$ M (mg)	20	20	20
Chitosan (mg)	200	200	200
Sodium tripolyphosphate (mg)	40	40	40
Kappa carrageenan (mg)	25	45	85

#### 2.4. Scanning Electron Microscopy (SEM)

Scanning electron microscopy (Model SU3500 SEM; Hitachi, Tokyo, Japan) was used to examine the morphology of  $\alpha$ M-Ch/Cr nanoparticles. Briefly,  $\alpha$ M-Ch/Cr nanoparticles were placed into the stub and were coated with platinum (30 s, 10 mA). The photomicrographs of  $\alpha$ M-Ch/Cr nanoparticles were observed at a 10 kV with differential magnifications ( $\times 10,000$ – $50,000$ ). Data were analyzed using ImageJ software (Madison, WI, USA) and Origin software (version 8.5, Northampton, MA, USA) to obtain the average particle size and distribution [30].

#### 2.5. Entrapment Efficiency and Drug Loading

The  $\alpha$ M-Ch/Cr entrapment efficiency and drug loading of nanoparticles were estimated by UV–VIS spectroscopy. Briefly, 25 mg sample of nanoparticles were added to ethyl acetate and the solution was centrifuged (3000 rpm, 10 min). Next, the supernatant was collected and the absorption at 245 nm was measured with an UV–visible spectrophotometer using a standard curve to obtain the amount of free  $\alpha$ M. Then, the sediment was resuspended in an appropriate volume of ethanol to determine the drugs that were encapsulated to find the total amount of  $\alpha$ M. To obtain the standard curve, different concentrations (2–12  $\mu$ g/mL) of  $\alpha$ M with serial dilution method were prepared and measured at 245 nm. The entrapment efficiency and drug loading of  $\alpha$ M in  $\alpha$ M-Ch/Cr nanoparticles were determined by the following Equations (1) and (2) [30].

$$\text{Entrapment efficiency (\%)} = \frac{\text{weight of the } \alpha\text{M in nanoparticle}}{\text{weight of } \alpha\text{M used}} \times 100\% \quad (1)$$

$$\text{Drug loading (\%)} = \frac{\text{weight of the } \alpha\text{M in nanoparticle}}{\text{weight of } \alpha\text{M nanoparticle}} \times 100\%. \quad (2)$$

#### 2.6. Fourier-Transform Infrared Spectroscopy (FTIR)

The interaction between  $\alpha$ M, chitosan (Ch), sodium tripolyphosphate (Tpp), kappa carageenan (Cr), and  $\alpha$ M-Ch/Cr nanoparticles was characterized using a Fourier-transform infrared spectrophotometer (Model IR Prestige-21; Shimadzu, Kyoto, Japan) with vacuum pressure (60 kN within 15 min) and measured at  $4000$ – $400$   $\text{cm}^{-1}$  [30,31].

#### 2.7. X-ray Diffraction (XRD)

The molecular arrangements of the  $\alpha$ M-Ch/Cr nanoparticle system were observed using x-ray diffraction (X-pert MPD diffractometer type, Rigaku International, Tokyo, Japan). The XRD patterns were collected over the angular range ( $2\theta$ ) of  $5$ – $60^\circ$ , with the generator set to 30 mA and 40 kV. The same condition was used for raw material analysis [30,32].

#### 2.8. Differential Scanning Calorimetry (DSC)

The thermal behavior of all raw materials and  $\alpha$ M-Ch/Cr nanoparticles was studied by differential scanning calorimetry (DSC-60; Mettler Toledo, Barcelona, Spain) and analyzed using TA-60WS software (Mettler Toledo, Barcelona, Spain). All measurements were performed at temperatures from  $30$  to  $300$   $^\circ\text{C}$ , with a heating rate of  $20$   $^\circ\text{C}/\text{min}$  under nitrogen flow [30,33].

#### 2.9. Saturation Solubility Study

The  $\alpha$ M-Ch/Cr nanoparticles were put into 5 mL distilled water pH 7.4, then constantly stirred for approximately 24 h. The sample was then filtered and diluted at a ratio of 1:3. Then, the  $\alpha$ M level was measured using a UV–VIS spectrophotometer at a wavelength of 245 nm [34].

### 2.10. In Vitro Drug Release

The  $\alpha$ M-Ch/Cr nanoparticle release profiles at pH 7.4 in phosphate buffered saline (PBS) and at a pH of 1.2 in a hydrochloric acid (HCl) solution were studied. Typically, 25 mg of  $\alpha$ M-Ch/Cr nanoparticles were suspended in PBS (pH 7.4) and in HCl solution (pH 1.2) in separate containers. Then, a 5 mL sampling was collected at each time interval of 5, 10, 15, 30, 45, and 60 min followed by the addition of fresh media. Furthermore, measurements were taken using a spectrophotometer instrument at a wavelength of 245 nm and the percent of drug released at each time interval was calculated [35].

### 2.11. In Vitro Cytotoxicity

The cell cytotoxicity of  $\alpha$ M, Ch-TPP,  $\alpha$ M-Ch, and  $\alpha$ M-Ch/Cr on MCF-7 cells were determined using MTT assay. Briefly, cells were seeded in a 96-well plate at a seeding density of  $5 \times 10^3$  cells/well and allowed to attach for 24 h. The following day, media was removed and replaced with a fresh one containing the different samples at varying concentrations (2:12  $\mu$ g/mL). Cells were incubated for 24 h. Media were removed and replaced with MTT solution at a concentration of 0.5 mg/mL and incubated for an additional 2–4 h at 37 °C. Next, 100  $\mu$ L SDS in 0.01% HCl was added and incubated in a dark place at room temperature overnight. The absorbance of the formed formazan was measured at 450 nm using ELISA Reader (Epoch™ Microplate Spectrophotometer, BioTek, Winooski, VT, USA). The cell viability was presented as a percentage of the control cells not exposed to the samples, as shown in Equation (3), and median inhibitory concentrations (IC<sub>50</sub>) were calculated from the dose–response curves [36]:

$$\text{Cell viability (\%)} = \frac{\text{absorbance at 450 nm of treated sample}}{\text{absorbance at 450 nm of control sample}} \times 100. \quad (3)$$

### 2.12. Statistical Analysis

Statistical analysis was completed using the Student's *t*-test. *p*-Values less than 0.05 were considered to be significant. Data are presented as mean  $\pm$  SD, *n* = 3 independent treatments.

## 3. Results

### 3.1. Characterization of Nanoparticles

#### 3.1.1. SEM, Particle Size, Entrapment Efficiency, and Drug Loading

The SEM images of the  $\alpha$ M-Ch/Cr nanoparticles are shown in Figure 2. Upon morphological characterization of the three  $\alpha$ M-Ch/Cr nanoparticle formulas, it was observed that all formulations formed spherical shapes. The particle size, entrapment efficiency, and drug loading of the polymeric nanoparticles are shown in Figure 3 and Table 2. In this study formula (2) was selected for further characterization and cytotoxic testing against MCF-7 breast cancer cells.

**Table 2.** The mean entrapment efficiency and drug loading of the nanoparticles.

Formulae	Entrapment Efficiency (%)	Drug Loading (%)
F1	98.74 $\pm$ 1.20	6.93 $\pm$ 0.87
F2	99.35 $\pm$ 1.10	6.51 $\pm$ 0.86
F3	98.59 $\pm$ 0.98	5.72 $\pm$ 0.60

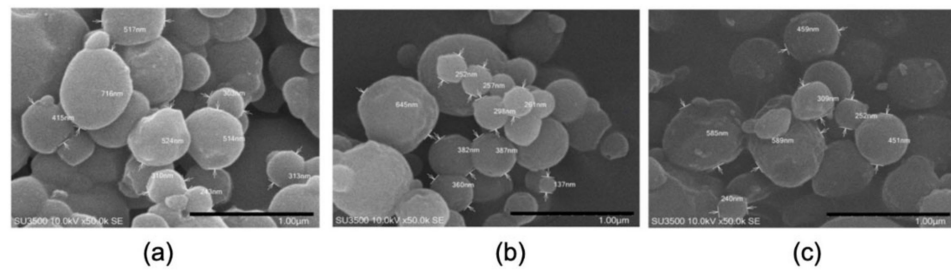


Figure 2. SEM images of (a) F1, (b) F2, and (c) F3.

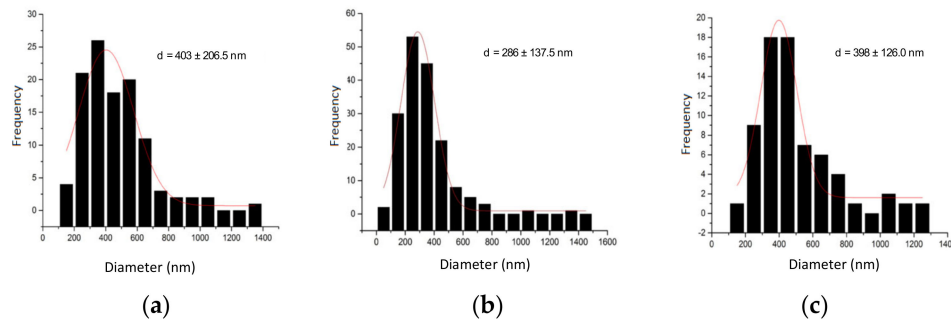


Figure 3. SEM size distribution analysis of (a) F1, (b) F2, and (c) F3.

### 3.1.2. FTIR Analysis

The FTIR spectrum of  $\alpha$ M, Ch, Tpp, Cr, and  $\alpha$ M-Ch/Cr nanoparticles are shown in Figure 4a and the data wavenumber of  $\alpha$ M, Ch, Tpp, and Cr are shown in Table 3. The spectrum of  $\alpha$ M-Ch/Cr nanoparticle showed the overlapping response of O–H and N–H at  $2400\text{ cm}^{-1}$ , C–H stretch at  $2900\text{ cm}^{-1}$ , N–H bend at  $1600\text{ cm}^{-1}$  from  $\alpha$ M and Ch, 3,6-anhydrogalactose at  $929\text{ cm}^{-1}$ , and C–O stretch at  $1076\text{ cm}^{-1}$  from Cr.

Table 3. FTIR wavenumber and corresponding functional groups.

Material	Wavenumber ( $\text{cm}^{-1}$ )		Functional Groups	Reference
	Result	Literature		
$\alpha$ -mangostin	34,081; 32,204	3260	O–H stretch	[37]
	29,875; 26,078; 29,317	2989; 2962; 2924	C–H stretch	
	16,338	1642	C=O	
	14,435	1454	C–C	
	11,782	1199	Ortho–OCH <sub>3</sub> stretch	
	107,533	1076	C–O–C stretch	
Chitosan	350,954	347,868	O–H stretch dan N–H stretch	[38]
	289,424	292,413	C–H stretch	
	165,302	165,688	C=O	
	1597	157,105	N–H bend	
	141,963	142,253	C–H bend	
	137,816	137,816	C–N	
	115,731	115,731	C–O–C stretch	
	1079	102,518	C–O	
Sodium tripolyphosphate	121,132	1210	$\nu_{as}$ P=O	[39]
	115,731	1130	$\nu_s$ O–P=O	
	109,269	1090	$\nu_{as}$ PO <sub>3</sub>	
	88,823	888	$\nu_{as}$ P–O–P	
Kappa carrageenan	1262	1241	O=S=O	[40]
	1069	1069	Glycosidic bond	
	929	922	3,6-anhydrogalactose	
	846	847	Galactose-4-sulfate	

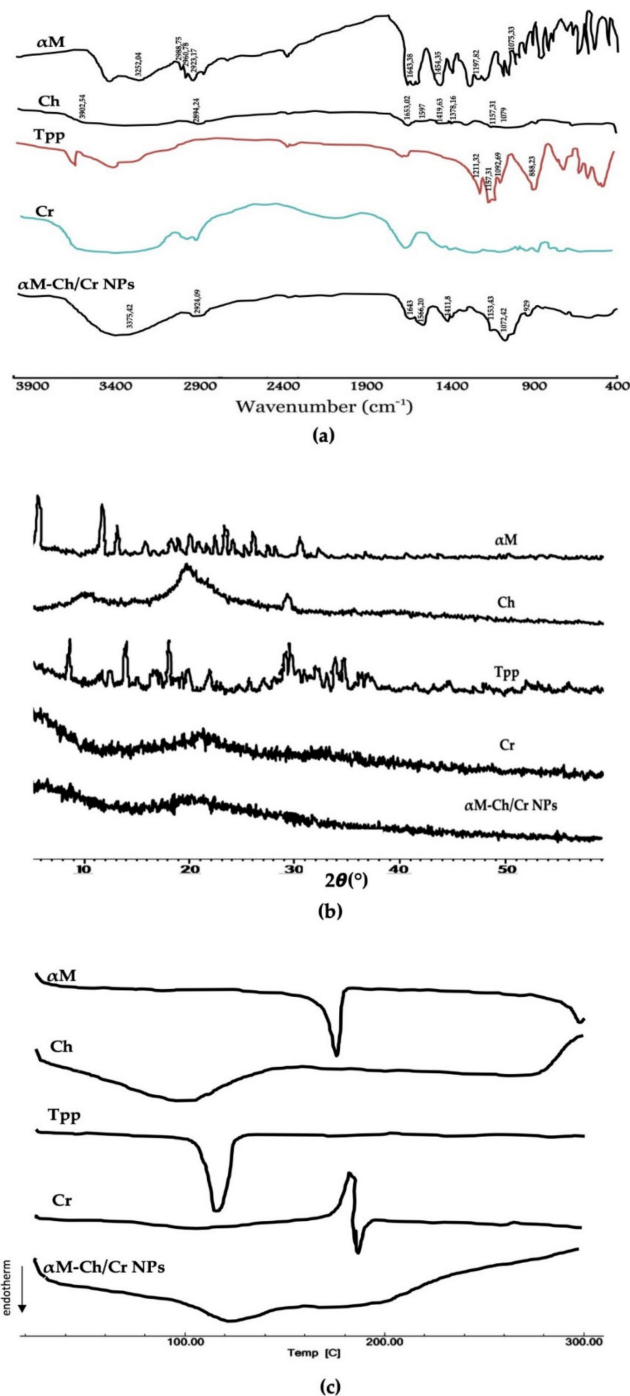


**Figure 4.** (a) FTIR spectra, (b) X-ray patterns, and (c) DSC thermograms of  $\alpha$ -mangostin, chitosan, carrageenan, and  $\alpha$ M-Ch/Cr nanoparticles.

### 3.1.3. XRD Analysis

The results of the XRD analysis can be seen in Figure 4b. Crystalline patterns from diffractogram data are shown by  $\alpha$ M and TPP with sharp diffractogram peaks from  $2\theta$  angles of 7–32°, semi-crystalline patterns are shown by chitosan at  $2\theta$  angle of 19.72° and amorphous patterns are shown by kappa carrageenan. The XRD results of  $\alpha$ M-Ch/Cr nanoparticles demonstrated an amorphous pattern.

### 3.1.4. DSC Analysis

The results of the DSC analysis are illustrated in Figure 4c. The DSC thermograms for  $\alpha$ M and TPP show the peaks of the endothermic phase at 178 and 120.06 °C. Ch appears to

provide a wide response signal that peaks around 100 °C. The  $\alpha$ M-Ch/Cr nanoparticles show patterns following the glass transition pattern, and the endothermic or exothermic peaks of crystalline component components such as  $\alpha$ M and TPP are no longer visible.

### 3.2. In Vitro Studies

#### 3.2.1. Saturation Solubility Study

Saturation solubility study results are shown in Figure 5a. In this study, an increase in the value of  $\alpha$ M solubility was four times that of the  $\alpha$ M-Ch/Cr nanoparticles (2.98–11.94  $\mu$ g/mL).

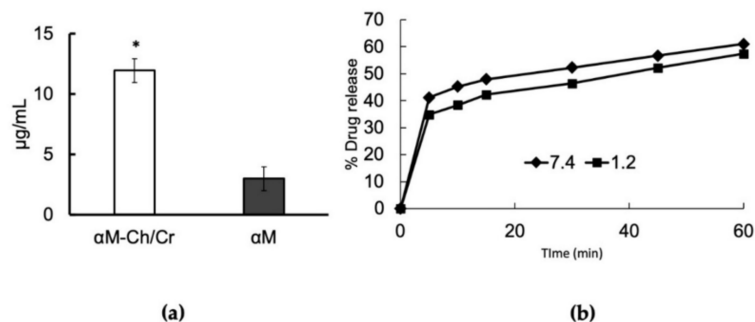


**Figure 5.** (a) Saturation solubility study of  $\alpha$ M and  $\alpha$ M-Ch/Cr nanoparticle and (b) release profiles at (■) pH 1.2 and (◆) pH 7.4 of  $\alpha$ M from  $\alpha$ M-Ch/Cr nanoparticle. Data represent mean  $\pm$  SD. \*  $p < 0.05$ , compared to  $\alpha$ M ( $p < 0.05$ ).

#### 3.2.2. In Vitro Release

The  $\alpha$ M-Ch/Cr nanoparticle in vitro release was evaluated in PBS (pH 7.4) and hydrochloric acid solution (pH 1.2) over a period of 60 min. The release profile of  $\alpha$ M-loaded nanoparticles exhibited an initial burst release of 34% and 42% for pH 1.2 and 7.0, respectively, over the first 5 min and then followed by a slow and sustained release over a period of 60 min (Figure 5b).

#### 3.2.3. In Vitro Cytotoxicity

For the in vitro cytotoxicity study, the cytotoxicity of Ch-TPP,  $\alpha$ M,  $\alpha$ M-Ch, and  $\alpha$ M-Ch/Cr nanoparticles were investigated after incubation with MCF-7 cells for 24 h (Figure 6). No cytotoxic effect on cells was observed for Ch-TPP. There was a significant difference between the cytotoxicity of  $\alpha$ M,  $\alpha$ M-Ch, and  $\alpha$ M-Ch/Cr nanoparticles. The IC<sub>50</sub> of  $\alpha$ M,  $\alpha$ M-Ch, and  $\alpha$ M-Ch/Cr was 8.2, 6.7, and 4.7  $\mu$ g/mL, respectively.

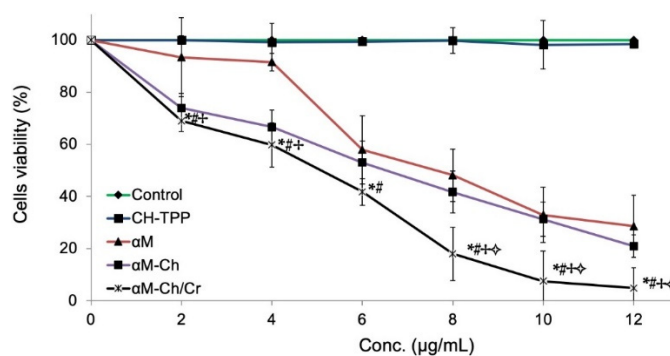


**Figure 6.** In vitro cytotoxicity of  $\alpha$ -mangostin,  $\alpha$ M-Ch, and  $\alpha$ M-Ch/Cr in MCF-7 cells based on the MTT assay. Data represent mean  $\pm$  SD. \*  $p < 0.05$ , compared to the control. #  $p < 0.05$ , compared to the CH-TPP. +  $p < 0.05$ , compared to the  $\alpha$ M. †  $p < 0.05$ , compared to the  $\alpha$ M-Ch.

#### 4. Discussion

This study aims to develop an orally administered nanoparticle polymeric system of  $\alpha$ -mangostin as a chemotherapy drug for breast cancer. The polymeric nanoparticles, using chitosan as a carrier and kappa carrageenan as a coating agent, were prepared using the ionic gelation method and spray pyrolysis.

Scanning electron microscopic imaging of the three  $\alpha$ M-Ch/Cr nanoparticle formulas revealed spherical nanoparticles. From the particle size, entrapment efficiency, and drug loading of polymeric nanoparticles (Table 2), it can be seen in each formula that there is no real correlation between variations of kappa carrageenan concentration and particle size or entrapment efficiency. Generally, particle size is strongly influenced by the concentration of material in each system, wherein the particle size will be larger for formula that contains a greater amount of ingredients [41]. However, there are certain conditions where there is no relationship between the amount of ingredients and the particle size. This could be due to the unevenness of the frequency of exposure received by the nanoparticle system at the time of manufacture to affect its size, as well as factors such as stirring speed, duration of stirring, duration of ultrasonication, temperature, and system pH [42]. In addition, this pattern can also be caused by the physicochemical properties of some polymers that have a strong attractive interaction with other particles due to the large surface free energy or high affinity for water molecules, which can cause fluid, osmotic, and thermodynamic imbalances that cause agglomeration of particles [43,44], so that the particle size obtained does not provide a clear pattern of relationship between its effect on the concentration of the material. Furthermore, the kappa carrageenan concentration in the formula affects drug loading, where the higher kappa carrageenan concentration will produce a smaller drug loading.

The size of the particles for cancer therapy drug delivery systems plays an important role, it can affect cellular uptake through the process of endocytosis and determines its fate during systemic circulation. In particular, particles with sizes ranging from 100 to 200 nm have the advantage of targeted delivery in cancer compared to those of larger sizes [45]. This is an additional justification for choosing formula 2 for further evaluation to determine its characteristics and cytotoxicity.

The  $\alpha$ M-Ch/Cr nanoparticle shows similar transmission peaks to those of Cr, with an absorption band at the wave number  $2400\text{ cm}^{-1}$  indicating the overlapping response of the hydroxy group and amine (OH and NH), aliphatic hydrocarbons (CH)  $2900\text{ cm}^{-1}$ , NH bending from the primary amine at  $1600\text{ cm}^{-1}$ , interactions between ammonium ions and phosphate  $1500\text{ cm}^{-1}$ ; carrageenan-specific functional groups were also observed at a peak of  $929\text{ cm}^{-1}$  indicating the presence of 3.6 anhydrogalactose groups; and glycosidic bonds were observed in areas around  $1076\text{ cm}^{-1}$ . The data indicate that the  $\alpha$ -mangostin was successfully loaded into nanoparticles system.

The diffractogram data for  $\alpha$ M-Ch/Cr nanoparticle demonstrates the amorphous pattern, or the transformation of crystalline or semicrystalline phases from the material component to amorphous is seen. The crystalline lattice of  $\alpha$ M is no longer visible, which indicates that  $\alpha$ M has been dispersed evenly in the nanoparticle matrix and encapsulated in the nanoreservoir system. In addition, the semi-crystalline change from chitosan is assumed to be due to the termination of the amine and hydroxy groups, which results in the formation of amorphous complexes with polymer encapsulators. This is also supported by DSC thermograms that shows the existence of endothermic phase peaks at  $178.00$  and  $120.06\text{ }^{\circ}\text{C}$  as the melting points of  $\alpha$ M and TPP. The pattern also illustrates that both materials are crystalline. Although Ch demonstrated a glass transition pattern, which indicates an amorphous shape, DSC thermograms showed an endothermic peak around  $100\text{ }^{\circ}\text{C}$ . This is the response from the  $\text{H}_2\text{O}$  evaporation phase, which is bound in a heat-induced chitosan molecule [46]. The  $\alpha$ M-Ch/Cr nanoparticles also show patterns following the glass transition pattern, and the endothermic or exothermic peaks of crystalline components such as  $\alpha$ M and TPP are no longer visible. Based on the correlation with XRD as seen in previous

tests, it was proved that  $\alpha$ M-Ch/Cr nanoparticles were molecularly dispersing  $\alpha$ M in the nanoparticle matrix system and encapsulated in the nanoreservoir system.

The  $\alpha$ M-Ch/Cr nanoparticles showed a 4-fold increase in the solubility value, likely due to the contribution of hydrophilic polymers used in the formula and also the nature of nanoparticles, which tend to increase the total surface area of the substance in contact with the solvent medium, resulting in a significant increase in solubility [47–49].

The in vitro release profile of  $\alpha$ M from  $\alpha$ M-Ch/Cr nanoparticles provides an extended-release pattern, due to the role of kappa-carrageenan, which is known to be able to control the drug release through the swelling mechanism. The dissolution process of nanoparticles occurs when they come in contact with the solvent medium forming cavities that act as the entry point for the solvent into the system and then dissolve the active substance. These then partition slowly out of the nanoreservoir system and provide an extended-release profile [50]. Based on the drug release curve, a burst release profile of 34% and 42% for pH 1.2 and 7.0, respectively, can be seen over the first 5 min and then followed by a controlled release over a period of 1 h. Burst release profiles are assumed to be due to the presence of  $\alpha$ M on the surface of the nanoparticles, which are immediately released when the nanoparticles are in contact with the solvent medium [51]. In addition, there was no significant difference between the release profiles in medium with two different pH conditions. This is due to the nature of carrageenan, which is not a pH-sensitive polymer but rather a thermal-sensitive polymer [25]. In fact, it can be seen that the value of  $\alpha$ -mangostin released at pH 1.2 tends to be lower than at pH 7.0 supporting another point of view about the ability of carrageenan in protecting the main carrier system of chitosan from protonation reaction mediated by gastric fluid.

In vitro cytotoxicity evaluation showed that the cell growth treated with the same anticancer concentration but in different formulations shows a different inhibitory response to the growth of cancer cells. When MCF-7 cells were treated with a dose of 2 and 4  $\mu$ g/mL of  $\alpha$ M in various formulations,  $\alpha$ M showed less cell growth inhibition compared to those formulated in the form of nanoparticles ( $\alpha$ M-Ch and  $\alpha$ M-Ch/Cr).

The use of biopolymers or a combination of excipients derived from nature often has the advantage to prevent drug efflux reactions that can reduce drug levels in the cytoplasm of cells [52], in contrast to those without using a combination, in general, drugs will be considered as foreign substances, which in the regulation will be released by the cell defense system, causing ineffective drug use [53]. The impressive results are shown by the formula encapsulated with carrageenan polymer, which shows an increase in cytotoxicity of  $\alpha$ M in inhibiting the growth of cancer cells. This is because carrageenan is known to have an influence on the regulation of cancer cells. Previous studies have shown that carrageenan can inhibit the migration of MDA-MB-231 breast cancer cells [54]. In addition, carrageenan has also been investigated for its anticancer activity in human cervical carcinoma cells (HeLa) and human umbilical vein endothelial cells (HUVEC); these studies show that carrageenan has activity in the specific cell cycle phase of human cervical carcinoma cells [55]. Carrageenan mechanism in inhibiting the growth of cancer cells has also been investigated, where carrageenan is able to induce the process of apoptosis through activating the pathways of caspase-3, caspase-8, and caspase-9; remodulation of the Bax:Bcl-2 ratio; and DNA damage [56]. This is probably what causes an increase in the cytotoxicity of  $\alpha$ M encapsulated with kappa carrageenan polymer against MCF-7 breast cancer cell lines.

## 5. Conclusions

In summary,  $\alpha$ M-Ch/Cr nanoparticles were successfully formulated and evaluated for their anticancer potential in MCF-7 breast cancer cells.  $\alpha$ M-Ch/Cr nanoparticles showed increased solubility of  $\alpha$ M-Ch/Cr, and the in vitro release test showed a sustained release pattern. In addition, the cytotoxicity study confirmed that  $\alpha$ M-Ch/Cr  $\alpha$ M has increased the cytotoxicity of  $\alpha$ M in MCF-7 breast cancer cells. These results suggest that  $\alpha$ M-Ch/Cr

nanoparticles have the potential to improve the physicochemical properties and cytotoxicity effects of  $\alpha$ M compounds as a candidate for breast cancer therapy agents.

**Author Contributions:** Conceptualization, N.W. and Y.H.; methodology, N.W.; validation, N.W., M.M., and Y.H.; formal analysis, A.R.; investigation, A.R., D.T., and Y.H.; writing—original draft preparation, A.R.; writing—review and editing, N.W., K.M., C.P., I.M.J., A.F.A.M., R.L., and M.M.; visualization, A.R. and L.M.; supervision, N.W.; project administration, L.M.; funding acquisition, N.W. All authors have read and agreed to the published version of the manuscript.

**Funding:** This research was funded by The Minister of Education and Culture, Republic of Indonesia, grant number (1827/UN6.3.1/LT/2020) and Rector of Universitas Padjadjaran for Academic Leadership Grant (1427/UN6.3.1/LT/2020).

**Institutional Review Board Statement:** Not applicable.

**Informed Consent Statement:** Not applicable.

**Data Availability Statement:** Samples of the data are provided by the corresponding author on request.

**Conflicts of Interest:** The authors declare no conflict of interest.

## References

1. Bray, F.; Ferlay, J.; Soerjomataram, I.; Siegel, R.L.; Torre, L.A.; Jemal, A. Global Cancer Statistics 2018: GLOBOCAN Estimates of Incidence and Mortality Worldwide for 36 Cancers in 185 Countries. *CA Cancer J. Clin.* **2018**, *68*, 394–424. [[CrossRef](#)] [[PubMed](#)]
2. Nounou, M.I.; Elamrawy, F.; Ahmed, N.; Abdelraouf, K.; Goda, S.; Syed-Sha-Qhattal, H. Breast Cancer: Conventional Diagnosis and Treatment Modalities and Recent Patents and Technologies Supplementary Issue: Targeted Therapies in Breast Cancer Treatment. *Breast Cancer Basic Clin. Res.* **2015**, *9*, 17–34. [[CrossRef](#)]
3. Ganoth, A.; Merimi, K.C.; Peer, D. Overcoming Multidrug Resistance with Nanomedicines. *Expert Opin. Drug Deliv.* **2015**, *12*, 223–238. [[CrossRef](#)] [[PubMed](#)]
4. Moiseenko, F.; Volkov, N.; Bogdanov, A.; Dubina, M.; Moiseyenko, V. Resistance Mechanisms to Drug Therapy in Breast Cancer and Other Solid Tumors: An Opinion. *F1000Research* **2017**, *6*, 1–8. [[CrossRef](#)]
5. Benjakul, R.; Kongkanermit, L.; Sarisuta, N.; Moongkarndi, P.; Müller-Goymann, C.C. Cytotoxic Effect and Mechanism Inducing Cell Death of  $\alpha$ -Mangostin Liposomes in Various Human Carcinoma and Normal Cells. *Anti-Cancer Drugs* **2015**, *26*, 824–834. [[CrossRef](#)]
6. Kritsanawong, S.; Innajak, S.; Imoto, M.; Watanapokasin, R. Antiproliferative and Apoptosis Induction of  $\alpha$ -Mangostin in T47D Breast Cancer Cells. *Int. J. Oncol.* **2016**, *48*, 2155–2165. [[CrossRef](#)]
7. Verma, R.K.; Yu, W.; Shrivastava, A.; Shankar, S.; Srivastava, R.K.  $\alpha$ -Mangostin-Encapsulated PLGA Nanoparticles Inhibit Pancreatic Carcinogenesis by Targeting Cancer Stem Cells in Human, and Transgenic (KrasG12D, and KrasG12D/Tp53R270H) Mice. *Sci. Rep.* **2016**, *6*, 1–13. [[CrossRef](#)]
8. Samprasit, W.; Akkaramongkolporn, P.; Jaewjira, S.; Opanasopit, P. Design of Alpha Mangostin-Loaded Chitosan/Alginate Controlled-Release Nanoparticles Using Genipin as Crosslinker. *J. Drug Deliv. Sci. Technol.* **2018**, *46*, 312–321. [[CrossRef](#)]
9. Wang, J.J.; Zeng, Z.W.; Xiao, R.Z.; Xie, T.; Zhou, G.L.; Zhan, X.R.; Wang, S.L. Recent Advances of Chitosan Nanoparticles as Drug Carriers. *Int. J. Nanomed.* **2011**, *6*, 765–774. [[CrossRef](#)]
10. Mohammed, M.A.; Syeda, J.T.M.; Wasan, K.M.; Wasan, E.K. An Overview of Chitosan Nanoparticles and Its Application in Non-Parenteral Drug Delivery. *Pharmaceutics* **2017**, *9*, 53. [[CrossRef](#)]
11. Pridgen, E.M.; Alexis, F.; Farokhzad, O.C. Polymeric Nanoparticle Technologies for Oral Drug Delivery. *Clin. Gastroenterol. Hepatol.* **2014**, *12*, 1605–1610. [[CrossRef](#)]
12. Hassani, S.; Laouini, A.; Fessi, H.; Charcosset, C. Preparation of Chitosan-TPP Nanoparticles Using Microengineered Membranes—Effect of Parameters and Encapsulation of Tacrine. *Colloids Surf. Physicochem. Eng. Asp.* **2015**, *482*, 34–43. [[CrossRef](#)]
13. Luppi, B.; Bigucci, F.; Abruzzo, A.; Corace, G.; Cerchiara, T.; Zecchi, V. Freeze-Dried Chitosan/Pectin Nasal Inserts for Antipsychotic Drug Delivery. *Eur. J. Pharm. Biopharm.* **2010**, *75*, 381–387. [[CrossRef](#)] [[PubMed](#)]
14. Samprasit, W.; Opanasopit, P. Chitosan-Based Nanoparticles for Controlled-Release Delivery of  $\alpha$ -Mangostin. *Int. J. Pharma Med. Biol. Sci.* **2020**, *9*, 1–5. [[CrossRef](#)]
15. Taher, F.A.; Ibrahim, S.A.; El-Aziz, A.A.; Abou El-Nour, M.F.; El-Sheikh, M.A.; El-Husseiny, N.; Mohamed, M.M. Anti-Proliferative Effect of Chitosan Nanoparticles (Extracted from Crayfish *Procambarus Clarkii*, Crustacea: Cambaridae) against MDA-MB-231 and SK-BR-3 Human Breast Cancer Cell Lines. *Int. J. Biol. Macromol.* **2019**, *126*, 478–487. [[CrossRef](#)] [[PubMed](#)]
16. Abedia, Z.; Moghadamnia, A.A.; Zabihi, E.; Pourbagher, R.; Ghasemi, M.; Nouri, H.R.; Tashakorian, H.; Jenabian, N. Anticancer Properties of Chitosan against Osteosarcoma, Breast Cancer and Cervical Cancer Cell Lines. *Casp. J. Intern. Med.* **2019**, *10*, 439–446. [[CrossRef](#)]

17. Jiang, Z.; Han, B.; Li, H.; Yang, Y.; Liu, W. Carboxymethyl Chitosan Represses Tumor Angiogenesis in Vitro and in Vivo. *Carbohydr. Polym.* **2015**, *129*, 1–8. [[CrossRef](#)]
18. Bonferoni, M.C.; Gavini, E.; Rasso, G.; Maestri, M.; Giunchedi, P. Chitosan Nanoparticles for Therapy and Theranostics of Hepatocellular Carcinoma (HCC) and Liver-Targeting. *Nanomaterials* **2020**, *10*, 870. [[CrossRef](#)]
19. Ai, J.W.; Liao, W.; Ren, Z.L. Enhanced Anticancer Effect of Copper-Loaded Chitosan Nanoparticles against Osteosarcoma. *RSC Adv.* **2017**, *7*, 15971–15977. [[CrossRef](#)]
20. Adhikari, H.S.; Yadav, P.N. Anticancer Activity of Chitosan, Chitosan Derivatives, and Their Mechanism of Action. *Int. J. Biomater.* **2018**, *2018*, 27–38. [[CrossRef](#)]
21. Vivek, R.; Nipun Babu, V.; Thangam, R.; Subramanian, K.S.; Kannan, S. PH-Responsive Drug Delivery of Chitosan Nanoparticles as Tamoxifen Carriers for Effective Anti-Tumor Activity in Breast Cancer Cells. *Colloids Surf. B Biointerfaces* **2013**, *111*, 117–123. [[CrossRef](#)] [[PubMed](#)]
22. Mahmood, M.A.; Madni, A.; Rehman, M.; Rahim, M.A.; Jabar, A. Ionically Cross-Linked Chitosan Nanoparticles for Sustained Delivery of Docetaxel: Fabrication, Post-Formulation and Acute Oral Toxicity Evaluation. *Int. J. Nanomed.* **2019**, *14*, 10035–10046. [[CrossRef](#)]
23. Jonassen, H.; Kjoniksen, A.L.; Hiorth, M. Stability of Chitosan Nanoparticles Cross-Linked with Tripolyphosphate. *Biomacromolecules* **2012**, *13*, 3747–3756. [[CrossRef](#)] [[PubMed](#)]
24. Szymańska, E.; Winnicka, K. Stability of Chitosan-A Challenge for Pharmaceutical and Biomedical Applications. *Mar. Drugs* **2015**, *13*, 1819–1846. [[CrossRef](#)] [[PubMed](#)]
25. Li, L.; Ni, R.; Shao, Y.; Mao, S. Carrageenan and Its Applications in Drug Delivery. *Carbohydr. Polym.* **2014**, *103*, 1–11. [[CrossRef](#)] [[PubMed](#)]
26. Briones, A.V.; Sato, T. Encapsulation of Glucose Oxidase (GOD) in Polyelectrolyte Complexes of Chitosan-Carrageenan. *React. Funct. Polym.* **2010**, *70*, 19–27. [[CrossRef](#)]
27. Bulmer, C.; Margaritis, A.; Xenocostas, A. Encapsulation and Controlled Release of Recombinant Human Erythropoietin from Chitosan-Carrageenan Nanoparticles. *Curr. Drug Deliv.* **2012**, *9*, 527–537. [[CrossRef](#)]
28. Mahdavinia, G.R.; Karimi, M.H.; Soltaniniya, M.; Massoumi, B. In Vitro Evaluation of Sustained Ciprofloxacin Release from  $\kappa$ -Carrageenan-Crosslinked Chitosan/Hydroxyapatite Hydrogel Nanocomposites. *Int. J. Biol. Macromol.* **2019**, *126*, 443–453. [[CrossRef](#)]
29. Liu, Y.; Yang, J.; Zhao, Z.; Li, J.; Zhang, R.; Yao, F. Formation and Characterization of Natural Polysaccharide Hollow Nanocapsules via Template Layer-by-Layer Self-Assembly. *J. Colloid Interface Sci.* **2012**, *379*, 130–140. [[CrossRef](#)]
30. Wathoni, N.; Rusdin, A.; Febriani, E.; Purnama, D.; Daulay, W.; Azhary, S.Y.; Panatarani, C.; Joni, I.M.; Lesmana, R.; Keiichi, M.; et al. Formulation and Characterization of  $\alpha$ -Mangostin in Chitosan Nanoparticles Coated by Sodium Alginate, Sodium Silicate, and Polyethylene Glycol. *J. Pharm. Bioallied Sci.* **2019**, *20*, 1–9. [[CrossRef](#)]
31. Smith, B. *Fundamentals of Fourier Transform Infrared Spectroscopy*, 2nd ed.; CRC Press: Boca Raton, FL, USA, 2011. [[CrossRef](#)]
32. Zak, A.; Majid, W.; ME, A.; Yousefi, R. X-Ray Analysis of ZnO Nanoparticles by Williamson–Hall and Size–Strain Plot Methods. *Solid State Sci.* **2011**, *13*, 251. [[CrossRef](#)]
33. Sarmento, B.; Ferreira, D.; Veiga, F.; Ribeiro, A. Characterization of Insulin-Loaded Alginate Nanoparticles Produced by Ionotropic Pre-Gelation through DSC and FTIR Studies. *Carbohydr Polym.* **2006**, *66*, 1–7. [[CrossRef](#)]
34. Baka, E.; Comer, J.E.A.; Takács-Novák, K. Study of Equilibrium Solubility Measurement by Saturation Shake-Flask Method Using Hydrochlorothiazide as Model Compound. *J. Pharm. Biomed. Anal.* **2008**, *46*, 335–341. [[CrossRef](#)]
35. Singhvi, G.; Singh, M. In-Vitro Drug Release Characterization Models. *Int. J. Pharm. Stud. Res.* **2011**, *2*, 77–84.
36. CCRC. U. Standard Procedure of the Cytotoxic Test MTT Method. *Cancer Chemoprevention Res. Cent.* **2012**, *2*, 1–7.
37. Nelli, G.B.; Anand Solomon, K.; Kilari, E.K. Antidiabetic Effect of  $\alpha$ -Mangostin and Its Protective Role in Sexual Dysfunction of Streptozotocin Induced Diabetic Male Rats. *Syst. Biol. Reprod. Med.* **2013**, *59*, 319–328. [[CrossRef](#)] [[PubMed](#)]
38. Yasmeen, S.; Kabiraz, M.; Saha, B.; Qadir, M.; Gafur, M.; Masum, S. Chromium (VI) Ions Removal from Tannery Effluent Using Chitosan-Microcrystalline Cellulose Composite as Adsorbent. *Int. Res. J. Pure Appl. Chem.* **2016**, *10*, 1–14. [[CrossRef](#)]
39. Loutfy, S.A.; Salaheldin, T.A.; Ramadan, M.A.; Farroh, K.Y.; Abdallah, Z.F.; Eloahed, T.Y.A. Synthesis, Characterization and Cytotoxic Evaluation of Graphene Oxide Nanosheets: In Vitro Liver Cancer Model. *Asian Pac. J. Cancer Prev.* **2017**, *18*, 955–961. [[CrossRef](#)]
40. Mahmood, W.A.K.; Khan, M.M.R.; Yee, T.C. Effects of Reaction Temperature on the Synthesis and Thermal Properties of Carrageenan Ester. *J. Phys. Sci.* **2014**, *25*, 123–138.
41. Albanese, A.; Tang, P.S.; Chan, W.C.W. The Effect of Nanoparticle Size, Shape, and Surface Chemistry on Biological Systems. *Annu. Rev. Biomed. Eng.* **2012**, *14*, 1–16. [[CrossRef](#)]
42. Reineck, P.; Brick, D.; Mulvaney, P.; Bach, U. Plasmonic Hot Electron Solar Cells: The Effect of Nanoparticle Size on Quantum Efficiency. *J. Phys. Chem. Lett.* **2016**, *7*, 4137–4141. [[CrossRef](#)] [[PubMed](#)]
43. Alexander, S.; Eastoe, J.; Lord, A.M.; Guittard, F.; Barron, A.R. Branched Hydrocarbon Low Surface Energy Materials for Superhydrophobic Nanoparticle Derived Surfaces. *ACS Appl. Mater. Interfaces* **2015**, *8*, 660–666. [[CrossRef](#)] [[PubMed](#)]
44. Arvaniti, E.C.; Juenger, M.C.G.; Bernal, S.A.; Duchesne, J.; Courard, L.; Leroy, S.; Provis, J.L.; Klemm, A.; De Belie, N. Determination of Particle Size, Surface Area, and Shape of Supplementary Cementitious Materials by Different Techniques. *Mater. Struct.* **2015**, *48*, 3687–3701. [[CrossRef](#)]

45. Li, C.F.; Li, Y.C.; Chen, L.B.; Wang, Y.; Sun, L.B. Doxorubicin-Loaded Eudragit-Coated Chitosan Nanoparticles in the Treatment of Colon Cancers. *J. Nanosci. Nanotechnol.* **2016**, *16*, 6773–6780. [[CrossRef](#)]
46. Acosta-Ferreira, S.; Castillo, O.S.; Madera-Santana, J.T.; Mendoza-García, D.A.; Núñez-Colín, C.A.; Grijalva-Verdugo, C.; Villalderma, A.G.; Morales-Vargas, A.T.; Rodríguez-Núñez, J.R. Production and Physicochemical Characterization of Chitosan for the Harvesting of Wild Microalgae Consortia. *Biotechnol. Rep.* **2020**, *28*. [[CrossRef](#)]
47. Dickmann, R.S.; Strasburg, G.M.; Romsos, D.R.; Wilson, L.A.; Lai, G.H.; Huang, H. Particle Size, Surface Area, and Amorphous Content as Predictors of Solubility and Bioavailability for Five Commercial Sources of Ferric Orthophosphate in Ready-to-Eat Cereal. *Nutrients* **2016**, *8*, 129. [[CrossRef](#)]
48. Qian, S.; Heng, W.; Wei, Y.; Zhang, J.; Gao, Y. Coamorphous Lurasidone Hydrochloride-Saccharin with Charge-Assisted Hydrogen Bonding Interaction Shows Improved Physical Stability and Enhanced Dissolution with Ph-Independent Solubility Behavior. *Cryst. Growth Des.* **2015**, *15*, 2920–2928. [[CrossRef](#)]
49. Włodarski, K.; Sawicki, W.; Haber, K.; Knapik, J.; Wojnarowska, Z.; Paluch, M.; Lepek, P.; Hawelek, L.; Tajber, L. Physicochemical Properties of Tadalafil Solid Dispersions-Impact of Polymer on the Apparent Solubility and Dissolution Rate of Tadalafil. *Eur. J. Pharm. Biopharm.* **2015**, *94*, 106–115. [[CrossRef](#)]
50. Grenha, A.; Gomes, M.E.; Rodrigues, M.; Santo, V.E.; Mano, J.F.; Neves, N.M.; Reis, R.L. Development of New Chitosan/Carrageenan Nanoparticles for Drug Delivery Applications. *J. Biomed. Mater. Res. Part J. Soc. Biomater. Jpn. Soc. Biomater. Aust. Soc. Biomater. Korean Soc. Biomater.* **2010**, *92*, 1265–1272. [[CrossRef](#)]
51. Xu, Y.; Du, Y. Effect of Molecular Structure of Chitosan on Protein Delivery Properties of Chitosan Nanoparticles. *Int. J. Pharm.* **2003**, *250*, 215–226. [[CrossRef](#)]
52. Nabekura, T.; Yamaki, T.; Hiroi, T.; Ueno, K.; Kitagawa, S. Inhibition of Anticancer Drug Efflux Transporter P-Glycoprotein by Rosemary Phytochemicals. *Pharmacol. Res.* **2010**, *61*, 259–263. [[CrossRef](#)]
53. Kobayashi, M.; Tsujiuchi, T.; Okui, Y.; Mizutani, A.; Nishi, K.; Nakanishi, T.; Nishii, R.; Fukuchi, K.; Tamai, I.; Kawai, K. Different Efflux Transporter Affinity and Metabolism of <sup>99m</sup>Tc-2-Methoxyisobutylisonitrile and <sup>99m</sup>Tc-Tetrofosmin for Multidrug Resistance Monitoring in Cancer. *Pharm. Res.* **2019**, *36*, 18. [[CrossRef](#)] [[PubMed](#)]
54. Groult, H.; Cousin, R.; Chot-Plassot, C.; Maura, M.; Bridiau, N.; Piot, J.M.; Maugard, T.; Fruitier-Arnaudin, I.  $\Lambda$ -Carrageenan Oligosaccharides of Distinct Anti-Heparanase and Anticoagulant Activities Inhibit MDA-MB-231 Breast Cancer Cell Migration. *Mar. Drugs* **2019**, *17*, 140. [[CrossRef](#)] [[PubMed](#)]
55. Prasedya, E.S.; Miyake, M.; Kobayashi, D.; Hazama, A. Carrageenan Delays Cell Cycle Progression in Human Cancer Cells in Vitro Demonstrated by FUCCI Imaging. *BMC Complement. Altern. Med.* **2016**, *16*, 270. [[CrossRef](#)] [[PubMed](#)]
56. Murad, H.; Ghannam, A.; Al-Ktaifani, M.; Abbas, A.; Hawat, M. Algal Sulfated Carrageenan Inhibits Proliferation of MDA-MB-231 Cells via Apoptosis Regulatory Genes. *Mol. Med. Rep.* **2015**, *11*, 2153–2158. [[CrossRef](#)] [[PubMed](#)]